Photocatalytic Disinfection of Selected Waterborne Pathogens by Visible Light-Active Nano Iron-Doped TiO2 Obtained by a Sol–Gel Method

ACS APPLIED NANO MATERIALS

www.acsanm.org

Article

Photocatalytic Disinfection of Selected Waterborne Pathogens by Visible Light-Active Nano Iron-Doped TiO_2 Obtained by a Sol–Gel Method

Najeebullah Channa, Tanveer A. Gadhi, Francesca Stefania Freyria, Alessandro Chiadò, Nicola Blangetti, Nicoletta Ditaranto, and Barbara Bonelli*

Cite This: *ACS Appl. Nano Mater.* 2025, 8, 10066–10079

Read Online

ACCESS | Metrics & More | Article Recommendations | Supporting Information

ABSTRACT: Bacterial contamination in drinking water systems poses a serious health risk due to poor hygiene, human activities, and cross-contamination within the water supply. This study examines the potential of iron-doped titanium oxide nanometric powder (Fe-TiO_2) for the photocatalytic disinfection of Gram-negative *E. coli* and Gram-positive *S. aureus* under visible light. The Fe-TiO_2 photocatalyst, with an optimal nominal content of 2.5 wt % Fe, was synthesized using a surfactant-assisted sol–gel method, resulting in a mesoporous nanomaterial composed of anatase nanoparticles with a specific surface area of 123 m^2/g. A sample of undoped anatase TiO_2, obtained using the same sol–gel method and exhibiting a specific surface area of 116 m^2/g, was utilized to confirm the role of Fe-doping in disinfection. The nanopowders were characterized using X-ray diffraction, N_2 sorption at −196 °C, diffuse reflectance UV–vis spectroscopy, X-ray photoelectron spectroscopy, electrophoretic mobility measurements, high-resolution transmission electron microscopy combined with energy-dispersive X-ray spectroscopy, and field emission scanning electron microscopy. Photocatalytic disinfection tests were conducted using 1 and 0.5 g/L Fe-TiO_2 with varying initial bacterial concentrations, with 1 g/L yielding the most promising results under the experimental conditions employed. After 240 min of treatment with 1 g/L Fe-TiO_2, a 99.9% removal of both *E. coli* and *S. aureus* was achieved starting from a bacterial concentration of 1×10^6 CFU/mL. A 99.9% removal of *E. coli* and a 99.8% removal of *S. aureus* were achieved starting from 1×10^4 CFU/mL. The Fe-TiO_2 nanomaterial was effective against high concentrations of both bacteria under visible light. Reusability was studied by recovering the Fe-TiO_2 nanoparticles and assessing their performance over three cycles. The photocatalytic disinfection effectiveness of Fe-TiO_2 nanoparticles under visible light was validated using an actual tap water sample containing 167 CFU/mL *total coliforms* and 8 CFU/mL *E. coli*. The bacteria were photocatalytically inactivated within 30 min.

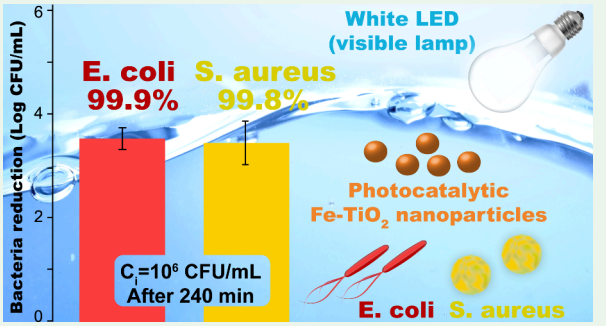

KEYWORDS: *photocatalysis, iron-doped TiO_2 nanoparticles, disinfection, E. coli, S. aureus, drinking water*

1. INTRODUCTION

The availability of clean water is a significant issue in low- and middle-income countries, where pollutants, particularly pathogenic bacteria, are present in drinking water systems and networks, leading to severe health problems for humans[1,2]Anthropogenic activities and cross-contamination in water bodies such as rivers, lakes, and ponds[3,4] from sewer lines are considered the primary sources of pathogens in the water supply distribution systems and the resulting waterborne diseases.[5−7]

The presence of various pathogenic bacteria in drinking water, such as *Salmonella* sp., *Shigella* sp., *V. cholera*, *P. aeruginosa*, *E. coli*, and *S. aureus*, can lead to serious health complications.[8−10]

Conventional water disinfection methods, such as UV light treatment, ozonation, and chlorination, are often expensive, may lead to the formation of toxic byproducts, and require proper technical attention in water treatment plants[11,12] Specifically, ozonation is quite costly and may produce carcinogenic byproducts in the treated water,[13] and the disinfection of pathogenic bacteria using high doses of chlorine can negatively impact human health and the environment.[14,15] Furthermore, some residual microbial contamination can still be found even after applying these treatments.[16] Therefore, alternative and effective water disinfection methods are

Received: March 12, 2025
Revised: March 28, 2025
Accepted: April 2, 2025
Published: April 9, 2025

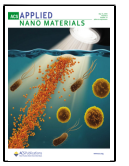

necessary to eliminate pathogenic bacteria. In this context, heterogeneous photocatalysis, a type of advanced oxidation process (AOP),[16] could enable the simultaneous inactivation of pathogenic bacterial cells and the degradation of other organic pollutants.

The use of photocatalysis for water disinfection is emerging as a promising alternative to conventional disinfection methods, particularly when sunlight can be exploited.[17] With increasing interest in photocatalytic disinfection, several authors are exploring the potential of new nanomaterials with upconversion and plasmonic properties, which can efficiently harness longer wavelength light in the visible and NIR ranges.[18,19]

TiO_2 is one of the widely used photocatalysts for water remediation,[20] alongside other semiconductors like ZnO. TiO_2-based photocatalysts can inactivate several Gram-negative and Gram-positive bacteria,[21] as well as degrade and even mineralize numerous organic contaminants at ambient temperature and pressure.[22,23]

The photocatalytic disinfection of *E. coli* and *S. aureus* using TiO_2 has been reported under UV light.[24] Indeed, one of the significant disadvantages of TiO_2 is its large band gap, necessitating the use of UV light, which constitutes a minor fraction of the solar spectrum. To address this limitation, doping with metals such as Fe, Cu, Zn, or Cd,[25−28] can decrease TiO_2 band gap, shifting its absorption edge toward the visible range. The lifetime of photogenerated electrons and holes is another drawback of TiO_2: metal doping (for instance, with Fe) can also enhance charge separation between holes (h^+) formed in the valence band and electrons (e^-) promoted to the conduction band.[29]

Among suitable heteroatoms for doping TiO_2, iron is the most abundant element on Earth overall and the fourth most abundant element in the crust[30]; it also plays a crucial role in several biological and chemical processes.[12] Fe-doped mesoporous TiO_2 nanoparticles, obtained in our laboratory through a direct doping method using surfactant-assisted sol−gel techniques, have demonstrated promising photocatalytic activity under simulated solar light for degrading phenol, a recalcitrant contaminant, and Acid Orange 7, a model molecule for nitrogen-containing organic pollutants.[31−33] The optimal Fe content was determined to be 2.5 wt %, because at higher Fe content, surface defects formed, resulting in undesired recombination of photogenerated charge carriers.[34]

Based on these results, this study reports the disinfection efficacy of Fe-doped TiO_2 nanoparticles (with a nominal iron content of 2.5 wt %) under visible light against two types of bacteria strains: Gram-negative *E. coli* and Gram-positive *S. aureus*.*E. coli* is commonly found in contaminated drinking water and food and is a leading cause of diarrhea and hemolytic uremic syndrome; *S. aureus* is a primary pathogen associated with hospital-acquired infections and quickly develops antibiotic resistance.[35−37]

Table S1 reports relevant literature on photocatalytic bacteria disinfection using Fe-doped TiO_2-based materials.[29,34,45−48,35,38−44] Several of these papers imply the fabrication of composites, the codoping of Fe-TiO_2 with other elements, or employing UV light for disinfection.[29,49]

Regarding the disinfection properties of Fe-doped TiO_2 under visible light, we found only two papers focused on powders[34,38] and two others on thin films.[35,46] Among these, only one paper suggests the use of Fe-doped TiO_2 against both *E. coli* and *S. aureus*: Yadav et al.[38] studied the photocatalytic disinfection of *E. coli* and *S. aureus* using 1−3 mol % Fe-TiO_2 (i.e., an Fe content comparable to the sample studied here) under the irradiation of eight fluorescent lamps (Philips TLD 8 W, λ mainly >400 nm with low emission in the near UV range). Khan et al.[34] investigated the inactivation of *E. coli* using 0.1 wt % Fe-TiO_2 under visible light irradiation using a halogen lamp 500 W at a light intensity of 30,798 lx.

We want to emphasize that the preparation method may significantly affect the surface and structural properties of Fe-doped TiO_2. The Fe content is only one factor to consider when evaluating photocatalytic efficiency, as other parameters, such as the type of TiO_2 polymorph, nanoparticle size, porosity, and surface composition, may also play a role.[31,32] From the photocatalytic perspective, anatase is regarded as one of the most active TiO_2 polymorphs, due to its high surface area and indirect band gap, which inhibits electron−hole recombination.[50] In this study, the photocatalysts were synthesized using a template-assisted sol−gel method, resulting in 100% anatase phase TiO_2 nanoparticles with a uniform size (approximately 10 nm, vide infra), high specific surface area, and effective Fe inclusion.[31−33] Another essential aspect of disinfection is that the rate can vary depending on the bacterial strains, likely because different bacteria possess different protection mechanisms.[51] Moreover, strains isolated from freshwater and wastewater exhibit greater resistance to AOPs than pure-type strains.[52] Pure strain tests are typically performed in defined solutions, such as saline solutions, known buffers, and culture media. However, actual water samples have different characteristics and contain various anions (Cl^-, F^-, NO_3^-, SO_4^{2-}, etc.) and metal cations (Ca^{2+}, Mg^{2+}, K^+, Zn^{2+}, Fe^{3+}, etc.) that could affect the performance of the chosen disinfection process.[53]

In addition, there is currently no recommendation regarding the concentration of the targeted microorganisms that would yield relevant outcomes easily applicable to real-life scenarios. Additionally, the bacterial load can vary from a few to 10^6 CFU/mL depending on the sampling point.[54] This variability is critical, as the amount of photocatalytic nanomaterial must be adjusted according to the starting concentration of the bacteria.[55] Typically, the initial bacterial concentration is determined based on the contamination level of tap water. *Total coliform, fecal coliform*, and *E. coli* are regarded as key indicators of contamination in aquatic environments.[56,57]

The tests were performed with two different starting concentrations of bacteria, 10^6 and 10^4 CFU/mL, to replicate two levels of contamination. In both scenarios, the rate of bacterial inactivation was monitored for at least 4 h using the colony count method, which is a commonly employed technique for determining the number of viable cells.[58]

Finally, to demonstrate the real applicability and potential of the nanomaterials, a sample of contaminated tap water was collected from a household in the Jamshoro region of Pakistan: the sample was microbiologically characterized and tested for its photocatalytic disinfection.

2. EXPERIMENTAL SECTION

2.1. Reagents. ACS-grade chemicals were used: most of the chemicals for the TiO_2 synthesis were acquired from Merck-Sigma-Aldrich (Schnelldorf, Germany); ethanol was acquired from Merck, Sigma-Aldrich (Italy), and sodium chloride (NaCl, 99.5%) from Daejung (Daejung chemicals and metals, China).

For bacterial analysis, Luria−Bertani broth (LB), Muller Hinton agar (MH), and RAPID' *E. coli* agar were acquired from Oxoid

https://doi.org/10.1021/acsanm.5c01408
ACS Appl. Nano Mater. 2025, 8, 10066−10079

Scheme 1. A Scheme of the Synthesis Procedure That We Adopted To Produce the Fe-TiO_2 Nanoparticles[45,54]

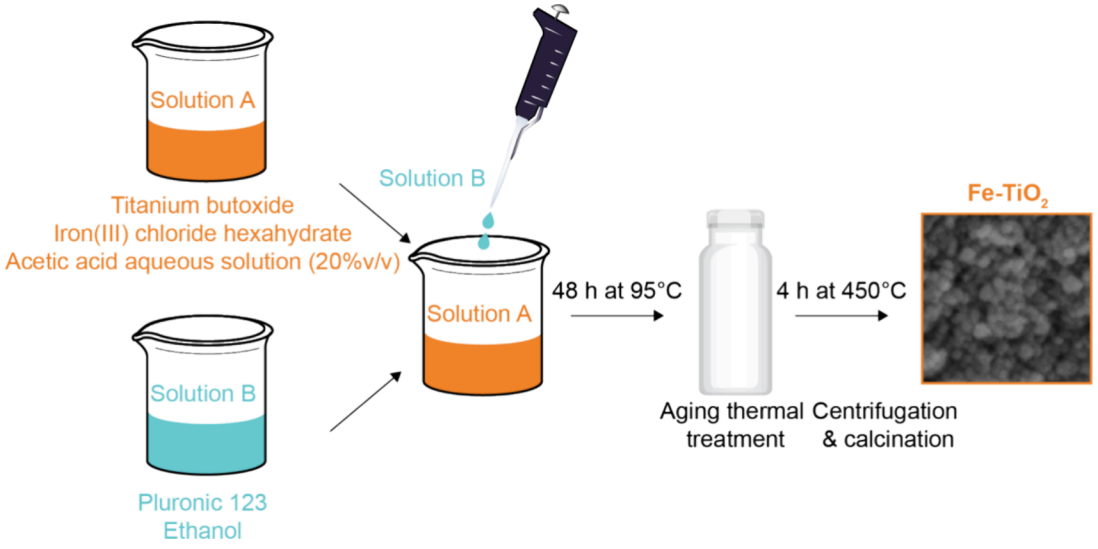

(England). To investigate cell damage, the LIVE/DEAD BacLight Bacterial Viability Kit was acquired from Thermo Fisher Scientific (USA).

2.2. Synthesis of Fe-Doped and Undoped TiO_2. A sample of TiO_2 with a nominal Fe content of 2.5 wt % (Fe-TiO_2) was synthesized using the method detailed in ref 32,33 and depicted in Scheme 1.

Two solutions (A and B) were initially prepared. Solution A was obtained by adding approximately 20. g of $Ti(OBut)_4$ (titanium butoxide) dropwise to 120 mL of a 20% v/v acetic acid solution with the addition of a nominal amount of $FeCl_3{\cdot}6H_2O$ (iron(III) chloride hexahydrate) corresponding to 2.5 wt % Fe. The solution was stirred for 4 h. Meanwhile, solution B was prepared by adding approximately 12 g Pluronic P123 (poly(ethylene glycol)-*block*-poly(propylene glycol)-*block*-poly(ethylene glycol)) to 80 mL of ethanol. Solution B was added dropwise to solution A and stirred continuously for 24 h at room temperature to produce a neat and transparent solution. Finally, the obtained mixture was transferred into a Teflon autoclave for hydrothermal treatment at 95 °C for 48 h. The resulting precipitate was centrifuged at 8,000 rpm for 15 min and washed twice with ethanol and water. Afterward, it was dried at 80 °C in a static stove and then calcined in air at 450 °C for 4 h (heating and cooling rate: 1.8 °C/min). A sample of undoped TiO_2 was synthesized using the same procedure, omitting the addition of $FeCl_3{\cdot}6H_2O$.

2.3. Physicochemical Characterization of the Powders. The phase composition and crystallinity of the powders were analyzed by collecting their X-ray diffraction (XRD) patterns on an X'Pert Philips PW3040 (Panalytical, Almelo, Netherlands). The X'Pert High Score Plus 3.0e software (Malvern Panalytical Ltd., Malvern, UK) was used to analyze the patterns.

N_2 adsorption/desorption isotherms were measured at −196 °C on nanopowders that had been previously outgassed at 150 °C to eliminate water and other atmospheric contaminants (Quantachrome Autosorb 1C, Boyton Beach, FL, USA). The Specific Surface Area (SSA) of the samples was obtained using the BET (Brunauer−Emmett−Teller) method. The Barrett−Joyner−Halenda (BJH) method was applied to the desorption branch of the isotherm for P/P^0 values exceeding 0.35 to determine the pore size distribution of the samples.

The diffuse reflectance (DR) UV−vis spectra of the samples were measured using a Varian Cary 5000 UV−Vis−NIR spectrophotometer (Agilent, Milan, IT) equipped with a DR sphere to analyze powders.

The surface chemical composition and speciation were analyzed using X-ray photoelectron spectroscopy (XPS) with a Versa Probe II scanning XPS microprobe spectrometer (Physical Electronics GmbH) equipped with a monochromatized Al K_α source (X-ray spot = 200 μm) at a power of 50.9 W. Both wide scans and high-resolution XP spectra were obtained using a fixed analyzer transmission (FAT) mode with pass energies of 117.40 and 29.35 eV, respectively. An electron gun facilitated charge compensation (1.0 V, 20.0 μA). All binding energy (BE) values were referenced to the C 1s line at 284.8 ± 0.1 eV for adventitious carbon. Data processing was completed using MultiPak software version 9.9.0.8.

The zeta potential of the nanopowders was measured using a Zetasizer Nano-ZS (Malvern Instruments, Worcestershire, UK). The nanoparticles were suspended in Milli-Q water and stirred magnetically for 5 min. Subsequently, the pH was adjusted by adding 0.1 M HCl or 0.1 M NaOH solutions.

The morphology of the nanopowders was investigated using electron microscopy techniques. Transmission Electron Microscopy (TEM) analysis was performed using a TALOS F200X (Thermo Scientific) microscope operated at 200 kV. TEM images were captured with a 16 Mpx CMOS camera (Ceta, Thermo Scientific). Scanning TEM (STEM) images were obtained on the same machine using an electron beam set at 200 kV and a current of approximately 25 pA in HAADF (High-Angle Annular Dark Field) mode.

Compositional maps were obtained using Energy Dispersive X-ray Spectroscopy (EDS). To achieve this, the probe current of the 200 kV electron beam was raised to approximately 750 pA. Simultaneously, the signal was collected by a 4-quadrant Silicon Drift Detector (SDD) and processed using the machine acquisition software (Velox, v. 3.10, Thermo Scientific) to extract elemental mapping. At least two maps for each sample were collected, and the corresponding EDS spectra were extracted from the entire map.

A Field Emission Scanning Microscope (FE-SEM) from MERLIN ZEISS AG, Oberkochen, Germany, was used to investigate further the morphology of the nanopowders (Figure S1).

The iron content in the Fe-TiO_2 nanopowder was measured using ICP/MS (Inductively Coupled Plasma Mass Spectrometry) on an ICAP Q (Thermofisher) before and after exposure to the bacteria cultures (vide infra). Approximately 10 mg of the sample was weighed and dissolved in a 25 mL solution. To aid dissolution, 2 mL of H_2SO_4 was added, and the mixture was heated in a beaker covered with a watch glass until white fumes appeared, ensuring complete dissolution. A four-point calibration curve was obtained using 100, 500, 1000, and 2000 ppb standards for quantification. The sample was subsequently diluted 10 or 50-fold before analysis.

2.4. Photocatalytic Disinfection Tests. *2.4.1. Preparation of the Bacterial Cultures.* *E. coli* (ATCC 8739)[59] and *S. aureus* (ATCC 25923)[60] were used. Initially, both bacteria were grown overnight in LB broth at 37 °C for 24 h.[61] Afterward, each bacterial mixture was centrifuged at 5,000 rpm for 15 min at 25 °C and washed three times

https://doi.org/10.1021/acsanm.5c01408
ACS Appl. Nano Mater. 2025, 8, 10066−10079

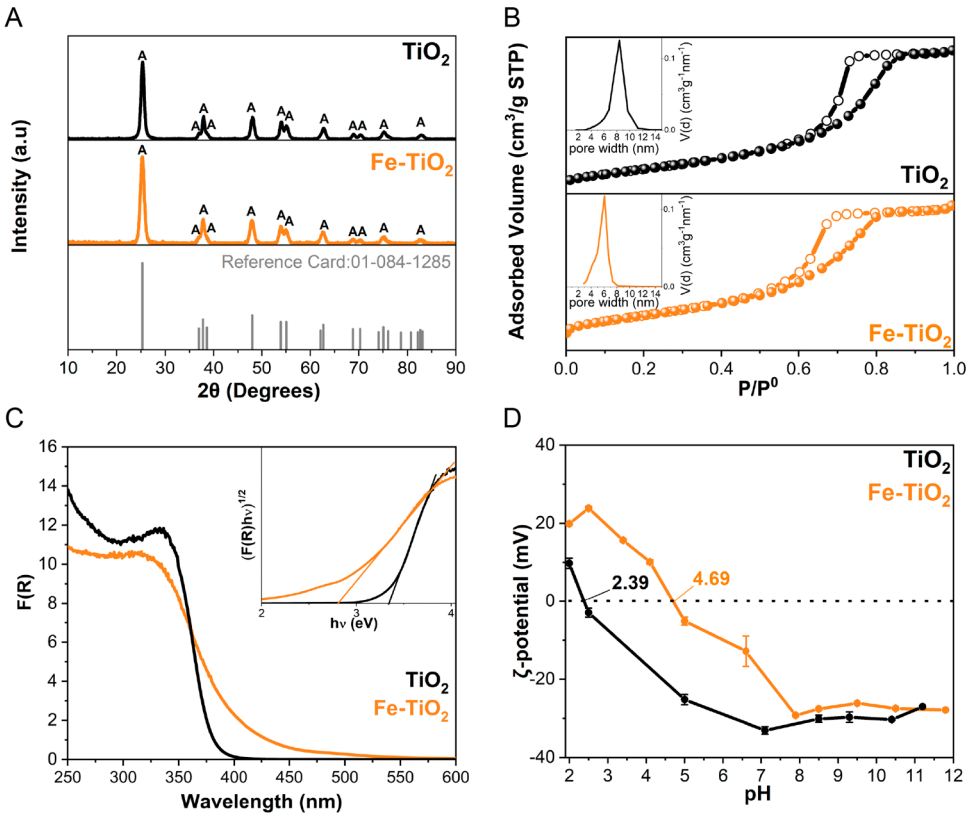

Figure 1. (A) XRD patterns of undoped TiO_2 (black line) and Fe-TiO_2 (orange line) nanopowders; the vertical bars correspond to the anatase peaks in the 01-084-1285 reference card. (B) N_2 adsorption/desorption isotherms at −196 °C of undoped TiO_2 (black line) and Fe-TiO_2 (orange line) nanopowders; full and empty symbols represent adsorption and desorption branches, respectively. The insets show the corresponding PSD, as determined by the BJH method; (C) DR UV−vis spectra of undoped TiO_2 (black line) and Fe-TiO_2 (orange line) nanopowders; the inset shows the corresponding Tauc's plot. (D) ζ-Potential curves based on electrophoretic mobility measurements versus pH of undoped TiO_2 (black line) and Fe-TiO_2 (orange line) nanopowders.

with normal saline solution (0.85% w/v). Finally, the bacterial concentration was assessed by optical density (OD) measurement at 600 nm. Then, the bacterial suspension was diluted to adjust the bacterial concentration to either 10^4 or 10^6 CFU/mL.[61] The plate count method, employed in most papers referenced in Table S1, validated the bacterial concentration.

2.4.2. Photocatalytic Disinfection of E. coli and S. aureus in Liquid Media. The photocatalytic disinfection experiments were performed with both strains at a relatively high bacterial load of 10^6 or 10^4 CFU/mL. Typically, 50 mg of Fe-TiO_2 was added to a beaker containing 50 mL of bacterial mixture (powder concentration of 1 g/L), and the suspension was stirred in the dark for 45 min. During the photocatalytic disinfection tests, the suspension was irradiated with a commercially available white LED lamp (Philips, 1535 lm, emission spectrum ranging from 430 to 800 nm) positioned approximately 45 cm from the bacteria solution[61] at room temperature (about 25 °C). In each experiment, after 0, 15, 30, 60, 90, 120, and 240 min, a 100 μL volume was withdrawn and serially diluted to 0.85% normal saline solution. Then, 100 μL of the diluted samples were spread on MH agar plates and incubated at 37 °C for twenty-4 h. After incubation, bacterial colonies were counted using a manual colony counter (Isolab, Germany) and reported in CFU/mL.

Three control experiments were included: (i) a "light control", involving the visible light irradiation of a bacterial suspension without any photocatalyst; (ii) a "dark control 1", involving the bacterial suspension and Fe-TiO_2 nanoparticles in the dark, and (iii) a "dark control 2" involving the bacterial suspension without photocatalyst in the dark. For brevity, the results of the "dark control 2" experiments will be reported in the SI.

To validate the antibacterial activity of Fe-TiO_2 under visible light, the experiments on the 10^6 CFU/mL mixtures (50 mL) were also conducted in the presence of 50 mg of undoped TiO_2 (nanopowder concentration of 1 g/L).

2.4.3. Reusability Tests. After the initial experiments, the reusability of Fe-TiO_2 was investigated. Three cycles were carried out with both bacterial strains to assess the stability and possible reuse of the nanomaterial. Initially, 80 mL of the bacterial and nanopowder mixture (with a powder concentration of 1 g/L) was stirred in a beaker for 45 min in the dark. Subsequently, the solution was irradiated under visible light.

After each cycle, the Fe-TiO_2 nanoparticles were collected and washed three times in total, twice with 70% ethanol solution and once with Milli-Q water, then centrifuged at 5000 rpm for 15 min at 25 °C to remove residual biomass and any viable remaining bacterial cells. Afterward, the nanoparticles were dried in an oven at 80 °C[62] for 5 h and then used for another inactivation test under the same conditions.

In each experiment, after 0, 120, and 240 min, a volume of 100 μL was withdrawn and serially diluted to 0.85% normal saline solution. Then, 100 μL of the diluted samples was spread on MH agar plates and incubated at 37 °C for 24 h. After incubation, bacterial colonies were counted and reported in CFU/mL.

2.4.4. Photocatalytic Disinfection Tests of Actual Tap Water Samples. The disinfection potential of Fe-TiO_2 nanoparticles under visible light was also tested with actual tap water collected from a household near Mehran University in Jamshoro, Pakistan. A tap water sample (approximately 1 L) was collected in a sterilized sample bottle and transported to the laboratory for further physicochemical and microbial analyses.

Initially, the total dissolved solids (TDS) and pH of the tap water were measured using portable instruments (Hanna EC/TDS meter Hi99301 and Hanna pH meter H18424). Sulfate and nitrate concentrations were analyzed using a UV−vis spectrophotometer

https://doi.org/10.1021/acsanm.5c01408
ACS Appl. Nano Mater. 2025, 8, 10066−10079

Table 1. Relevant Physicochemical Properties of the Samples

sample	average crystallite size (nm)[a]	SSA (m^2 g^{-1})[b]	V_{tot} (cm^3 g^{-1})[b]	pH_{IEP}[c]	bandgap energy (E_g, eV)[d]	valence band energy (VB, eV)[e]	conduction band energy (eV)[f]
undoped TiO_2	14 ± 3	116	0.18	2.39	3.34	2.60	−0.74
Fe-TiO_2	11 ± 3	123	0.21	4.69	2.80	2.30	−0.50

[a]As determined by applying the Debye-Scherr method to the XRD patterns. [b]As determined by N_2 sorption isotherms at −196 °C. [c]As determined by electrophoretic measurements. [d]As determined by applying Tauc's plot method for indirect semiconductors. [e]As determined by XPS. [f]Calculated as CB = VB − E_g.

(Shimadzu, 1800) following the 4500-SO_4^{2-} and 4500-NO_3^- standard methods recommended by the American Public Health Association (APHA). Chloride concentration and total hardness were measured in accordance with the guidelines of APHA standard methods.[63]

Specific agar (RAPID' *E. coli* agar) was used for the microbial analysis of *E. coli* and *total coliform*.[8,64] Initially, 100 mL of the tap water sample was passed through a membrane filter (mixed cellulose ester membrane, 0.45 μm); then, the filter was placed on an agar plate and incubated at 37 °C for 24 h. Afterward, the bacterial colonies were counted using a colony counter and reported as CFU/mL units.

Since the tap water sample showed some bacterial contamination (Table S2), 100 mL of tap water was mixed with 100 mg of Fe-TiO_2 to achieve the same concentration of 1 g/L of the experiments carried out with the bacterial strains in liquid media: the suspension was irradiated under visible light as reported in 2.4.2. After 15 min of stirring in the dark, photocatalytic disinfection was carried out under the LED lamp at room temperature.

To assess the bacterial disinfection, 1 mL of suspension (tap water and photocatalyst) was withdrawn at different time intervals of 0, 15, and 30 min, spread on specific RAPID' *E. coli* agar,[8] and incubated at 37 °C for 24 h. Finally, the bacterial colonies were counted using a manual colony counter and reported in CFU/mL.

2.4.5. Bacterial Cells Live/Dead Staining and Fluorescence Microscopy. Live/dead staining was carried out and analyzed by fluorescence microscopy to assess cell viability. Initially, 1 mL aliquots were withdrawn from the treated suspension at different intervals, followed by centrifugation at 10,000 × *g* for 10 min to obtain the bacterial pellets. The pellets were washed three times with a 0.85% normal saline solution, after which the supernatant was drained. Subsequently, the pellets were resuspended in 1 mL of 0.85% of NaCl and mixed. Then 5 μL of mixed dyes (SYTO 9 and propidium iodide (PI), 1:1(v:v)) was added to stain the bacterial suspension and incubated in the dark for 15 min at room temperature. Afterward, a 5 μL sample was pipetted onto a glass slide and analyzed using an Axio Scope A1 fluorescence microscope (Zeiss, Germany).[61]

3. RESULTS AND DISCUSSION

3.1. Physicochemical Characterization of the Undoped and Fe-Doped TiO_2 Powders. The crystalline phases of both Fe-TiO_2 and undoped TiO_2 were characterized using powders XRD. As shown in Figure 1A, for both powders, all observed peaks correspond to the TiO_2 anatase phase (reference PDF card: 01-084-1285). Consistent with our previous work on Fe-doped TiO_2 nanoparticles with similar Fe content,[31,32] XRD did not detect peaks ascribable to any crystalline Fe-containing phases, likely due to the low Fe content.

The average crystallite size, determined by applying Debye−Scherrer's method, was 11 ± 3 and 14 ± 3 nm for Fe-TiO_2 and undoped TiO_2, respectively. The slightly smaller crystallite size of the Fe-doped sample may be due to the presence of Fe, which inhibits crystallite growth, as previously reported in the literature.[32]

The N_2 sorption isotherms at −196 °C are shown in Figure 1B. Both powders exhibit type IV isotherms, characteristic of mesoporous materials with very limited microporosity[65] Both isotherms show an H2(b) hysteresis loop, which may result from some delayed condensation and desorption pore-blocking effects within inkbottle mesopores. The specific surface area (SSA) and total pore volume (V_{tot}) values are reported in Table 1: a slight increase in both values was observed with Fe-doping, alongside a decrease in the most probable pore size (inset to Figure 1B), as determined by the BJH method.

The DR UV−vis spectra obtained with the two nanopowders are shown in Figure 1C. With undoped TiO_2, the typical absorption band due to the O^{2-} to Ti^{4+} charge transfer transition is observed below 400 nm. In comparison to undoped TiO_2, the Fe-TiO_2 UV−vis spectrum shows (i) a red-shift of the absorption onset, due to Fe doping, and (ii) a broad absorption band at longer wavelengths (approximately 500 nm), ascribed to the *d*−*d* transition of Fe^{3+} ions in some surface Fe-oxyhydroxide species (FeO_xH_y), as already discussed in references.[31,32] The amount of such FeO_xH_y species is limited, and/or they are likely highly dispersed at the surface, ultimately eluding XRD detection.

The samples' bandgap was evaluated using Tauc's plot method for indirect semiconductors (i.e., by plotting $(F(R)*h\nu)^{1/2}$ versus Energy, eV) being anatase the only polymorph. The inset in Figure 1C shows the corresponding Tauc's plots from which band gap energy (E_g) values of 3.34 eV (λ_{max} = 371 nm) and 2.80 eV (λ_{max} = 443 nm) were extrapolated for undoped TiO_2 and Fe-TiO_2, respectively. These results suggest an improved light-capturing ability due to Fe-doping, which may lead to improved photocatalytic activity of Fe-TiO_2 in the visible range, attributed to both the red-shift of the bandgap and the presence of surface FeO_xH_y species that absorb in the visible range.

XPS enabled the measurement of the valence band (VB) energy position (spectra not shown). The corresponding values (Table 1) were employed to determine the CB position by considering the E_g values determined using DR UV−vis spectroscopy (CB = VB − E_g). In comparison to undoped TiO_2 (VB = 2.60 eV), the VB shifts to 2.30 eV, confirming Fe doping.[66]

The line shape of high-resolution Fe 2p XP spectrum of Fe-TiO_2 (Figure S2) was compared with the line shape of Fe^{3+} and Fe^{2+} containing compounds and underwent curve-fitting. The thick envelope and the absence of a shakeup feature between 2p3/2 and 2p1/2 peaks, along with the fitting results, suggested the copresence of both Fe^{3+} and Fe^{2+} ions. Due to the complex multiplet arising from the two oxidation states, Figure S2 reports a simplified curve fitting that emphasizes the presence of the peak component at BE = 709.4 ± 0.1 eV (main peak for Fe^{2+}) and that at BE = 710.9 ± 0.1 eV (main peak for Fe^{3+}). The component at 716 eV can be interpreted as both Fe^{3+} surface peak and Fe^{2+} shakeup.[67] The sampling depth of the XPS analysis (approximately 7−8 nm) allows for the investigation of surface and subsurface atomic layers. In this case, we can hypothesize that Fe-doping leads to the formation

https://doi.org/10.1021/acsanm.5c01408
ACS Appl. Nano Mater. 2025, 8, 10066−10079

Scheme 2. Possible Events Occurring under Visible-Light Illumination of the Studied Fe-TiO_2 Nanoparticles, Including the Formation of ROS and Subsequent Inactivation of *E. coli* and *S. aureus* Bacterial Cells

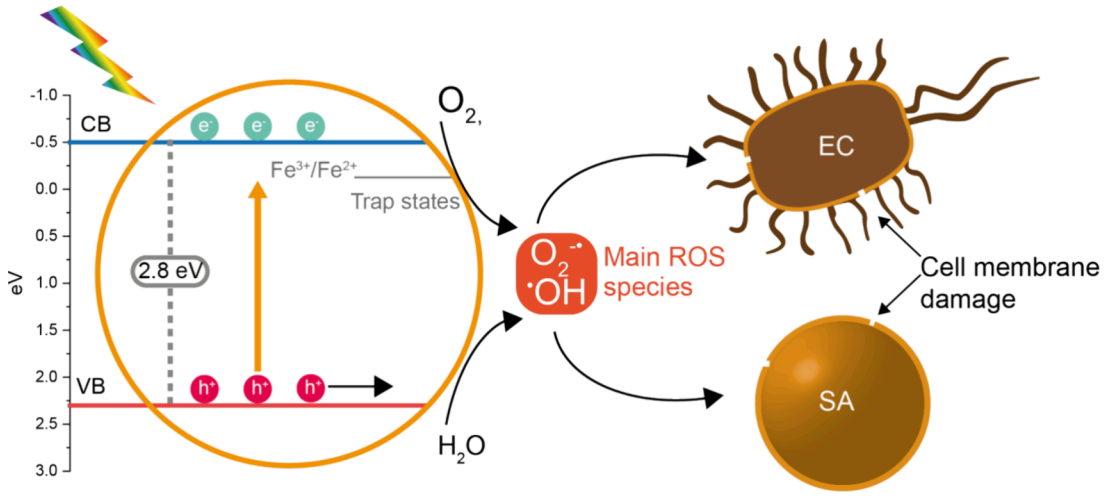

of certain defects, namely Fe^{2+} species, likely located beneath the very first atomic layers, which can also serve as trap sites (as depicted in Scheme 2). These same species could also contribute to the tail observed at longer wavelengths in the DR UV−vis spectrum of Fe-TiO_2.

Figure 1D presents the electrophoretic mobility measurements of the two powders, both exhibiting a negatively charged surface across a broad pH range. Interestingly, Fe-TiO_2 shows an increase of the pH at the isoelectric point (pH_{iep}), likely due to the presence of surface FeO_xH_y species detected by DR UV−vis spectroscopy (Figure 1C), which aligns with previous work.[32]

Figure 2A,B display two selected HRTEM micrographs of the studied nanopowders; both reveal the presence of roundish nanoparticles with a relatively uniform shape and size (in the 10−13 nm range), exhibiting some degree of agglomeration/aggregation. The HRTEM micrographs indicate a lattice spacing of 3.51 Å for both nanopowders, characteristic of the (101) plane of the anatase phase. Notably, the observed nanoparticles' size is comparable to the crystallite size determined by XRD, suggesting that the employed synthesis method produces monocrystalline nanoparticles. Furthermore, images captured in STEM mode (Figure 2C,D) demonstrate the presence of intraparticle porosity.

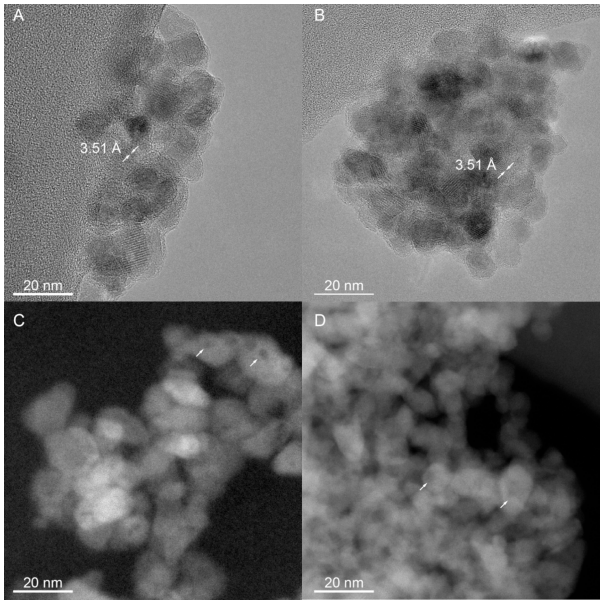

Figure 2. Selected HRTEM images in transmission (A, B) and STEM mode (C, D) of undoped TiO_2 (panels A and C) and Fe-TiO_2 (panels B and D).

Elemental analysis of the Fe-TiO_2 nanopowder by EDS (Figure S3) confirmed the presence of iron, with an average content of 2.56 wt % ± 0.41%. This aligns with the nominal amount (2.5 wt % Fe). The Fe content, measured by ICP-MS, confirmed the presence of iron at 2.44 wt % (Table S3). The slight discrepancy between the two values may relate to EDS being a semiquantitative technique, while the ICP-MS is a more reliable method for element quantification.

3.2. Photocatalytic Disinfection of *E. coli* and *S. aureus* in Liquid Media. Once characterized, Fe-TiO_2 was tested for the photocatalytic disinfection of selected bacterial strains (*E. coli* and *S. aureus*) at two different bacterial loads (10^6 and 10^4 CFU/mL) to simulate two relatively high levels of pathogens found in actual tap water samples. Indeed, although no bacteria should be detected in drinking water (the WHO-recommended threshold is 0 CFU/mL), there are several examples of contamination with bacterial loads ranging from a few to 10^6 CFU/mL.[54]

Figure 3A,B display the results of the disinfection experiments with an initial bacteria concentration of 10^6 CFU/mL for both *E. coli* and *S. aureus*. In the presence of the visible-light-activated nanomaterials, both strains demonstrated a dramatic decrease in viable bacterial cells (Figures S4 show images of some of the plates used for the counts). Similar results were previously achieved using Bi_2O_3 nanomaterial with the same bacterial strains using the same inoculum concentration, i.e., 10^6 CFU/mL.[61]

The Log reduction in relation to the initial bacterial concentration was calculated to assess the efficiency of bacterial inactivation. This value is generally used to compare the effects of various water treatment processes.[25] Notably, Fe-TiO_2 nanoparticles at a concentration of 1 g/L allowed for the reduction of viable bacteria to almost 10^2 CFU/mL after 240 min of visible light exposure, which corresponds to nearly a 99.97% reduction or 3.53 Log (3.57 ± 0.21 and 3.49 ± 0.42

https://doi.org/10.1021/acsanm.5c01408
ACS Appl. Nano Mater. 2025, 8, 10066−10079

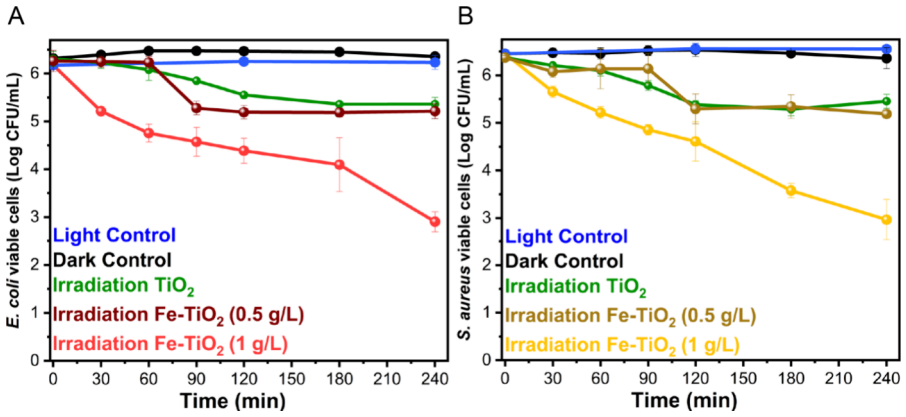

Figure 3. Evaluation of the viable CFU/mL over time (Log scale) for (A) *E. coli* in the presence of 1 g/L Fe-TiO_2 (red line), 0.5 g/L Fe-TiO_2 (dark red line), or 1 g/L undoped TiO_2 (green line) under visible light irradiation, and (B) *S. aureus* in the presence of 1 g/L Fe-TiO_2 (yellow line), 0.5 g/L Fe-TiO_2 (light brown line) and 1 g/L undoped TiO_2 (green line) under visible light irradiation. An initial bacterial concentration of 10^6 CFU/mL was employed. All the panels also depict the viable CFU/mL over time during the light control experiments (blue line, bacteria suspension without photocatalyst under visible light irradiation) and of the dark control 1 experiments (black lines, bacteria suspension in the presence of 1 g/L Fe-TiO_2 in the dark).

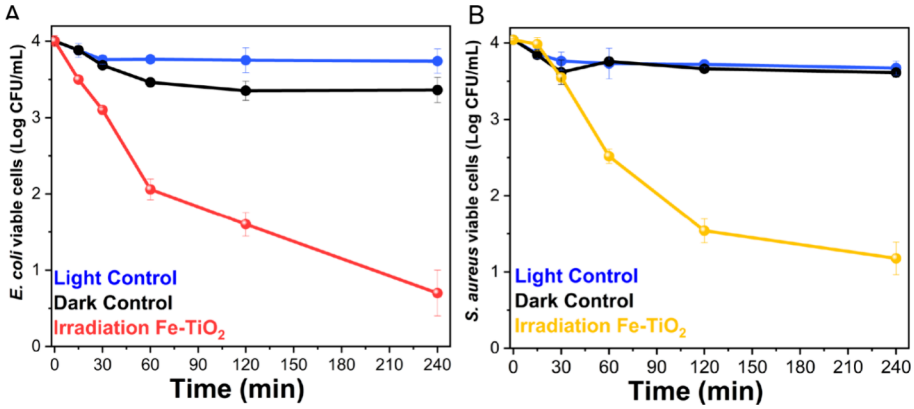

Figure 4. Evaluation of the viable CFU/mL over time (Log scale) for (A)*E. coli* and (B)*S. aureus* in the presence of 1 g/L Fe-TiO_2 (yellow line) under visible light irradiation. An initial bacterial concentration of 10^4 CFU/mL was used. All the panels also show the viable CFU/mL over time during the light control (blue line, bacteria suspension without photocatalyst under visible light irradiation) and dark control 1 (black line, bacterial suspension containing 1 g/L Fe-TiO_2 in the dark).

Log reductions for *E. coli* and *S. aureus*, respectively), whereas TiO_2 at the same concentration of 1 g/L concentration achieved less than 90% reduction (0.95 ± 0.14 and 0.92 ± 0.15 Log reductions for *E. coli* and *S. aureus*, respectively). Therefore, the Fe-doped nanomaterial was 2.6 times more effective than the undoped TiO_2 nanopowder, likely due to its absorption properties in the visible range, as identified by DR UV−vis spectroscopy. Conversely, the photocatalytic efficacy of undoped TiO_2 is limited under visible light, consistent with its optical properties.

The results from the control experiments support the hypothesis that these outcomes are primarily due to the photocatalytic behavior of the studied nanomaterials. The viable bacterial cells of both strains remained nearly stable in the light and dark controls throughout the entire test (the results of dark control 2 are reported in Figure S5) as nearly no growth or significant Log reduction was observed. Indeed, as illustrated in Figure 3, the light control (blue line) indicated no apparent effect (no growth promotion or inhibition) of visible light on the growth of both bacteria compared to dark control 2. Similarly, since dark control 1 allows for the evaluation of any potential toxic effects of the nanomaterial without light activation, the stable values of CFU/mL obtained during these control experiments confirm that the nanomaterial toxicity is negligible, and disinfection can only be achieved in the presence of the photocatalytic powder. For completeness, only a slight reduction (about 0.1 Log reduction) was observed for both dark controls concerning *S. aureus*. Consequently, the growth of this strain appears to be slightly reduced in the dark regardless of the presence of the photocatalytic nanomaterial. This effect is attributed to the strain's growth behavior in the presence of light and is likely negligible.

Furthermore, the photocatalytic efficiency in the inactivation of the same starting concentration of bacteria (10^6 CFU/mL) was monitored with both bacterial strains using a lower concentration of Fe-TiO_2 nanoparticles, namely 0.5 g/L. Figure 3 shows that this lower dose of Fe-TiO_2 nanoparticles resulted in decreased bacterial inactivation compared to experiments using 1 g/L. Indeed, only a 91% reduction, or 1.08 Log, was achieved (1.05 ± 0.05 and 1.12 ± 0.02 Log reductions for *E. coli* and *S. aureus*, respectively). Light control and dark control experiments were also carried out with the lower dose (0.5 g/L), and no significant Log reduction was observed (Figure S6). These results indicate that, under the

https://doi.org/10.1021/acsanm.5c01408
ACS Appl. Nano Mater. 2025, 8, 10066−10079

employed experimental conditions, a higher dose of nanomaterial is necessary, as 1 g/L of Fe-TiO_2 nanoparticles provides nearly three times more effective bacterial inactivation (3.4 and 3.1 for *E. coli* and *S. aureus*, respectively). Additionally, it is noteworthy that the decrease of viable bacteria at a lower concentration of Fe-TiO_2 nanoparticles is comparable to that achieved by 1 g/L undoped TiO_2.

Figure 4 presents the results of the disinfection experiments conducted with an initial bacteria concentration of 10^4 CFU/mL for both *E. coli* and *S. aureus*. Given the findings from tests with higher bacterial concentrations, which indicated significantly lower activity of undoped TiO_2, these photocatalytic tests were performed only with 1 g/L Fe-TiO_2. The results showed a 99.9% (Log 3.31 ± 0.10) reduction for*E. coli* and 99.8% (Log 2.82 ± 0.11) for*S. aureus* following 240 min of light exposure. The purpose of these tests was to evaluate the effectiveness of the nanomaterial in the presence of a lower yet still substantial bacterial load.

Over time, the evaluation of the viable bacterial cells revealed trends like those reported in Figure 3, demonstrating an effective reduction in both strains. The controls indicated a slight decrease in the number of viable cells. Under these conditions, the mere presence of visible light (light control, blue curves) suggests that a minor physiological decrease in viable cells should be noted. This effect is observable in both strains (0.28 ± 0.15 and 0.42 ± 0.10 Log reduction for *E. coli* and *S. aureus*, respectively), but it is negligible compared to the impact of light in the presence of the photocatalyst. Following an initial decrease, the count remained nearly constant until the test concluded (up to 240 min). Simultaneously, some effects of powder toxicity (dark control 1, black curves) were recorded with both strains. *E. coli* showed a 0.7 ± 0.15 Log reduction of viable cells when kept in the dark with the nanomaterial powder present. *S. aureus*, on the other hand, exhibited a smaller decrease of viable cells in the dark (0.5 ± 0.09 Log reduction) compared to the Gram-negative *E. coli*. This trend further confirms our observations from the irradiated condition in this test (Figure 4) as well as in previous tests with a higher starting concentration of viable cells (10^6 CFU/mL). At higher concentrations, viable cells were less affected by either the toxicity or photocatalytic properties of the nanometric powders, although these effects were still evident.

Then, the photocatalytic efficiency in inactivating the same initial concentration of bacteria (10^4 CFU/mL) was tested with a lower concentration of Fe-TiO_2 nanoparticles (0.5 g/L) using both bacterial strains. Once again, as shown in Figure S7, a lower dose of photocatalyst led to a reduced bacterial inactivation compared to the experiments carried out with 1 g/L. In fact, only a 92% reduction, or 1.22 Log, was reached (1.33 ± 0.13 and 1.12 ± 0.09 Log reductions for *E. coli* and *S. aureus*, respectively). However, the results indicate that at a higher dosage (1 g/L), the bacterial reduction is nearly three times greater as compared with a lower dosage (0.5 g/L). As illustrated in Figure S7, no such reduction was noted in the control tests at a lower dose (light control: blue curves, dark control 1: black curves). Furthermore, in this scenario, no toxic effects were recorded, as no difference in the viable bacterial amount is apparent in the dark control trend line.

It is important to note that the disinfection efficiency of Fe-TiO_2 is slightly higher against the Gram-negative *E. coli* than against the Gram-positive *S. aureus*, as expected, as clearly shown with a 10^4 CFU/mL starting concentration (Figure 4). A possible explanation is that this effect arises from the differing susceptibility of their cell membranes to the reactive oxygen species (ROS) produced during the photocatalytic process, as well as the unique characteristics of *S. aureus*. Indeed, it is known that ROS generated in aerated aqueous media during photocatalysis, mainly $^{\bullet}O_2^-$ (superoxide anions) and $^{\bullet}$OH (hydroxyl radicals) species, can penetrate and damage the cell membranes of bacteria, resulting in disinfection.[68,69] Compared to *E. coli*, *S. aureus* has a peptidoglycan cell wall and an external polysaccharide capsule that better protects the microorganism.[37] Additionally, it is catalase-positive;[36] making it more likely to survive the ROS generated during the photocatalytic treatment.

Scheme 2 shows the events that may lead to the photocatalytic inactivation of *E. coli* and *S. aureus* after the photoactivation of Fe-TiO_2 nanoparticles by visible light. Concerning the type of ROS present in our photocatalytic system, the photocatalytic behavior of the Fe-TiO_2 nanoparticles has been studied in the presence of various radical scavengers under the same experimental conditions (specifically, a photocatalyst concentration of 1 g/L and illumination with visible light).[61] It was found that superoxide species and positive holes (which trigger the formation of hydroxyl radicals in water) were the active species; thus, we expect that both $^{\bullet}O_2^-$ and •OH are the primary ROS contributing to the disinfection activity of Fe-TiO_2. Additionally, the presence of subsurface Fe^{2+} species (identified by XPS) strongly suggests that our synthesis procedure promotes the formation of Fe^{2+} species that, in turn, enhance the production of $\bullet O_2^-$ ions, besides •OH radicals. Under illumination, Fe-TiO_2 nanoparticles facilitate the formation of ROS naturally occurring in a nondeaerated aqueous phase. The visible light-activated Fe-TiO_2 nanomaterial significantly reduced the number of viable cells, even in the presence of the defense strategies of the targeted bacteria.

Comparison with existing literature is challenging because experiments using different powders are conducted under various reaction conditions. Nevertheless, we chose to make some reasonable comparisons with a selection of studies presented in Table S1, which were performed under the most comparable conditions to ours, specifically two papers analyzing Fe-doped TiO_2 powders with similar concentrations of photocatalyst (g/L) and bacteria (CFU/mL) under visible light.

For example, Yadav et al.[38] examined various concentrations of photocatalytic materials (0.1, 0.5, 1, and 2 g/L) at a light intensity of 0.5 mW/cm^2. They found that with 0.5 g/L of nanomaterial, only 60% of bacterial reduction was achieved after 240 min of treatment. In contrast, at 1 g/L, complete inactivation was reached, making it the most effective concentration. Indeed, increasing the photocatalytic dose beyond 1 g/L does not give any further advantage. Moreover, Khan et al.[34] applied the same photocatalyst dose (1 g/L) to inactivate *E. coli* with an initial concentration of 10^4 CFU/mL, attaining a 100% log reduction after 150 min. The faster disinfection they achieved is likely due to the higher intensity (500 W) of the visible light source used, compared to the intensity of our light source (7.3 W). On one hand, the results of bacterial inactivation reported here highlighted the significant efficiency of our Fe-TiO_2 nanoparticles under visible light. On the other hand, the lack of comparable data underscores the need for further studies on this subject.

https://doi.org/10.1021/acsanm.5c01408
ACS Appl. Nano Mater. 2025, 8, 10066−10079

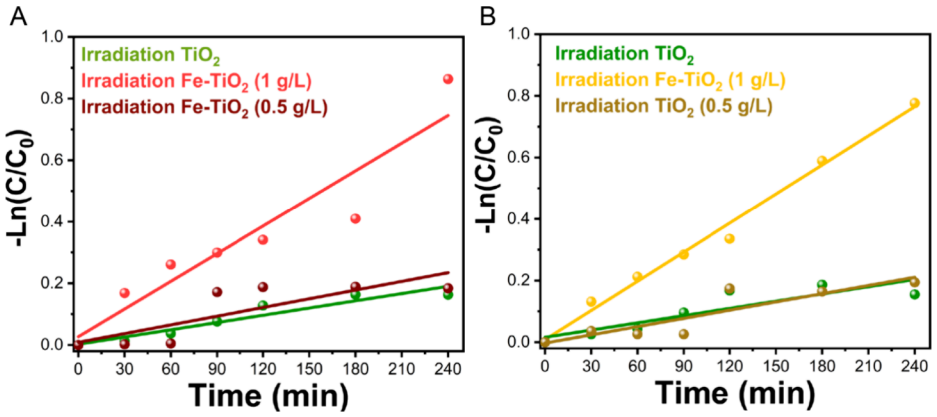

Figure 5. Kinetic curves of *E. coli* (A) and *S. aureus* (B) showing Log reduction under visible light irradiation in the presence of TiO_2 (1 g/L) and Fe-TiO_2 (1 and 0.5 g/L) with an initial bacterial concentration of 10^6 CFU/mL.

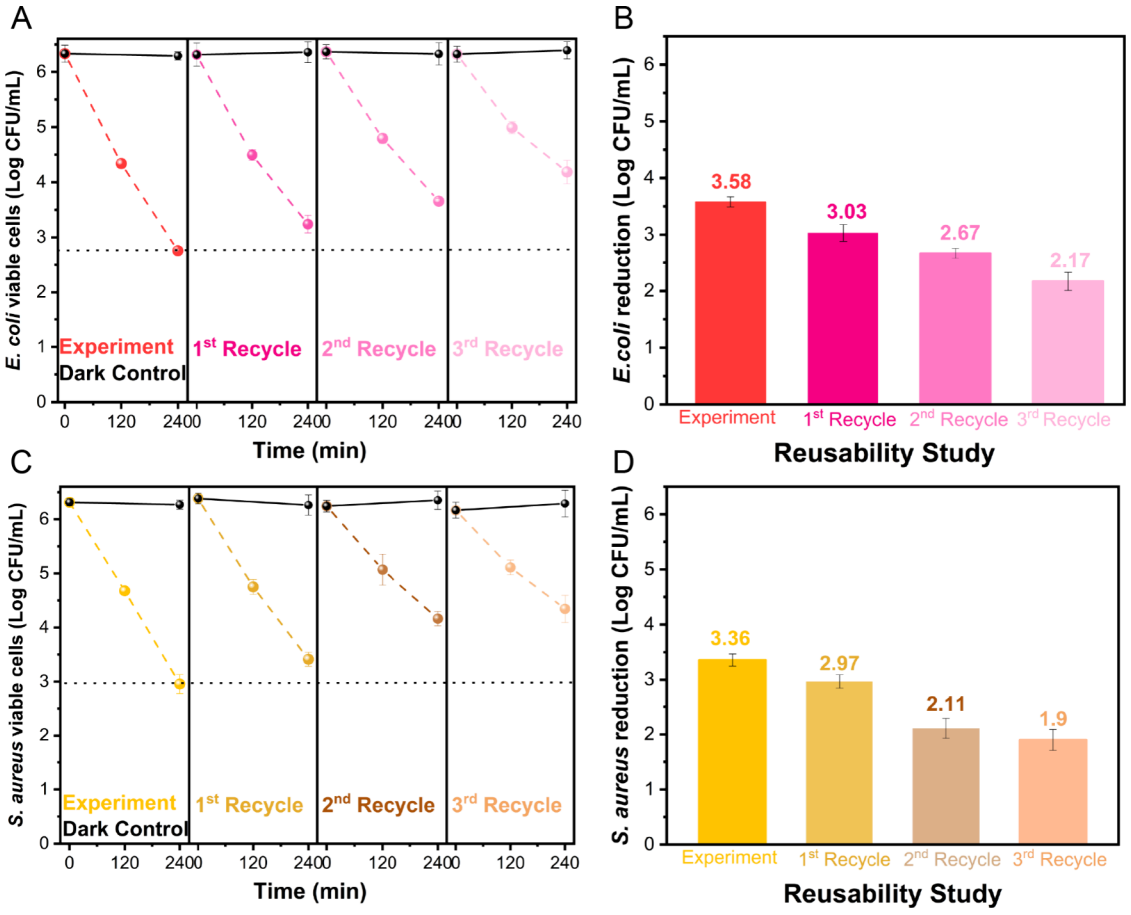

Figure 6. Reusability study of Fe-TiO_2 nanoparticles for up to three cycles following the initial inactivation of both bacteria strains. Panels (A) and (B) report, respectively, the viable CFU/mL (Log scale) of *E. coli* and the total Log reduction of *E. coli* after 240 min in each cycle. Panels (C) and (D) report, respectively, the viable CFU/mL (Log scale) of *S. aureus* and the total Log reduction of *S. aureus* after 240 min in each cycle. All tests conducted under visible light irradiation were performed with an initial bacterial concentration of 10^6 CFU/mL, in the presence of 1 g/L photocatalyst. The dark control 1 experiments (black lines) were carried out with a suspension containing 10^6 CFU/mL bacteria and 1 g/L Fe-TiO_2 in the dark.

The results obtained from these photocatalytic tests can be further investigated by examining the inactivation kinetics. Figure 5 reports the kinetics curves for disinfection with 10^6 CFU/mL bacteria concentrations achieved with 0.5 g/L Fe-TiO_2, 1 g/L Fe-TiO_2, and undoped TiO_2. With 1 g/L undoped TiO_2, the rates are nearly 3 times smaller than those obtained with 1 g/L Fe-TiO_2. For the undoped material, a rate of approximately $0.8 \times 10^{-3} \pm 0.1 \times 10^{-3}$ 1/min ($R^2 = 0.89$) was calculated for *E. coli* and $0.8 \times 10^{-3} \pm 0.2 \times 10^{-3}$ 1/min ($R^2 = 0.73$) for *S. aureus*. With 1 g/L Fe-TiO_2 rates of approximately $2.9 \times 10^{-3} \pm 0.5 \times 10^{-3}$ 1/min ($R^2 = 0.87$) and $3.1 \times 10^{-3} \pm 0.2 \times 10^{-3}$ 1/min ($R^2 = 0.98$) were calculated for *E. coli* and *S. aureus*, respectively. At the lower dosage of 0.5 g/L, Fe-TiO_2, a rate of approximately $0.9 \times 10^{-3} \pm 0.2 \times 10^{-3}$ 1/min (R^2 =

https://doi.org/10.1021/acsanm.5c01408
ACS Appl. Nano Mater. 2025, 8, 10066−10079

0.61) was calculated for *E. coli* and ca. $0.8 \times 10^{-3} \pm 0.2 \times 10^{-3}$ 1/min ($R^2 = 0.75$) for *S. aureus*, indicating a rate very similar to that achieved with 1 g/L of undoped TiO_2. For completeness, the kinetics for an initial bacterial concentration of 10^4 CFU/mL are shown in Figure S8, which reveals slopes demonstrating an even faster rate (nearly twice as fast) compared to 10^6 CFU/mL. Furthermore, comparing the slopes of the kinetic curves highlights the superior effectiveness of Fe-TiO_2 in disinfecting Gram-negative *E. coli* compared to Gram-positive *S. aureus*.

To confirm that the bacteria were effectively killed by the photocatalytic treatment, live/dead fluorescence staining was performed. In this test, cells with an intact membrane stain green with SYTO 9, while cells with a compromised membrane that are dead or dying stain red with propidium iodide. Figures S9 and S10 show the corresponding microscope images. These images reveal that initially, live, green-stained cells were observed for both strains. After 15 min, in the presence of visible light-activated Fe-TiO_2 nanoparticles, the number of red-stained cells increased, indicating bacterial inactivation. With prolonged exposure to the photocatalytic treatment, more red-stained bacterial cells of *S. aureus* and *E. coli* were observed in the case of Fe-TiO_2 nanoparticles, likely due to cell membrane damage caused by the photogenerated ROS. Some green-stained cells of *S. aureus* could be seen after 240 min, confirming incomplete bacterial inactivation. However, with *E. coli*, almost all the cells were red-stained after 240 min, indicating that the photocatalytic treatment was more effective against *E. coli* than *S. aureus*.

3.3. Results of the Reusability Study. Following the initial inactivation experiments, a study was conducted to examine the stability and reusability of the Fe-TiO_2 photocatalyst. Subsequently, after the initial tests of bacterial inactivation, the nanoparticles were recovered, as detailed in the experimental section, and reused for up to three cycles.

The bacterial inactivation efficiency, expressed as Log reduction, is shown in Figure 6. During the first recycling cycle, the bacterial inactivation of both strains was comparable to what is reported in Figure 3, and bacterial inactivation continued to be observed in each subsequent cycle. A slight reduction was noted in the following recycling tests for both strains (Figure 6A,C). Nevertheless, the maximum Log reduction (illustrated in the bar chart of Figure 6B,D) decreases after each cycle, with an overall decrease of 0.86 Log and 1.07 Log after three recycling tests for *E. coli* and *S. aureus*, respectively; specifically, the efficiency against *E. coli* and *S. aureus* was (slightly) reduced by approximately 7 and 10%, respectively. The dark controls (bacterial suspension and Fe-TiO_2 recycled nanoparticles in the dark) were also conducted in each recycling experiment, and no significant Log reduction was observed (Figure 6A,C, black lines).

Overall, the results of the reusability tests demonstrated that the Fe-TiO_2 photocatalyst could be recovered and recycled after liquid applications, indicating that it is also a quite stable material. ICP-MS analysis carried out on the recovered powder (Table S3) measured an overall Fe content of 2.26 wt % after the reusability tests with *E. coli* and 2.18 wt % with *S. aureus*, which is lower than the original amount, likely due to some Fe leaching phenomena that could occur during the repeated washing steps. In comparison to the initial ICP-MS-determined Fe content of 2.44 wt %, however, a total Fe leaching of 7 and 11% was recorded after the reusability tests with *E. coli* and *S. aureus*, respectively, suggesting that optimizing the recycling conditions could yield even better results.

3.4. Photocatalytic Disinfection of an Actual Water Sample. An actual tap water sample was utilized to validate the bacterial disinfection properties of the Fe-TiO_2 nanoparticles. The results of the analysis of the tap water sample are shown in Table S2, which includes the WHO's threshold guidelines on drinking water quality for comparison.[6,70] The physicochemical water quality parameters met WHO's standards. However, the water quality parameters related to microbial contamination exceeded the threshold limits, with 167 CFU/mL detected for *total coliforms* and 8 CFU/mL for *E. coli* alone. This bacterial contamination in tap water likely resulted from some cross-contamination between the sewer lines and the drinking water network system. In any event, *total coliform, fecal coliform,* and *E. coli* are regarded as indicators of microbial contamination in drinking water. Therefore, the collected tap water was tested in the presence of 1 g/L of Fe-TiO_2 nanoparticles to analyze the disinfection capability of this nanomaterial (Figure 7).

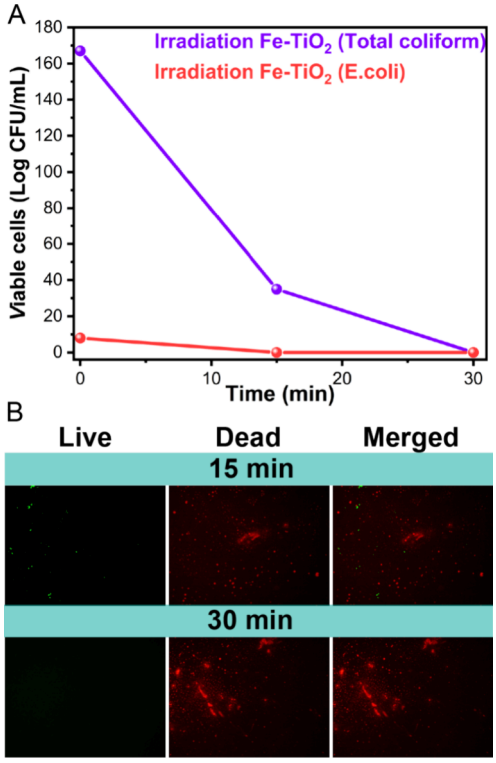

Figure 7. Photocatalytic disinfection of *E. coli* and *total coliforms* in an actual tap water sample (CFU/mL) using 1 g/L Fe-TiO_2 nanoparticles activated by visible light (A). Fluorescence microscopy images of the live/dead staining that were taken during the photocatalytic disinfection test of the tap water sample over time (B).

As shown in Figure 7A, 15 min of photocatalytic treatment led to a 0.9 Log (100%) reduction of *E. coli* and a 1.5 Log (77%) reduction of *total coliform*. After 30 min, a 100% reduction in *total coliforms* was observed. Selected fluorescence microscopy images related to the live/dead staining of samples taken during the test are presented in Figure 7B. After 15 min, a few green live cells coexist with some red dead cells, but after 30 min, no green fluorescence is visible, confirming extensive bacterial deactivation. Although the disinfection efficiency in

https://doi.org/10.1021/acsanm.5c01408
ACS Appl. Nano Mater. 2025, 8, 10066−10079

tap water samples may be slightly higher than that achieved during disinfection experiments at both bacterial loads (10^6 or 10^4 CFU/mL), due to the lower viable bacteria present in the sample compared to the very high bacterial load tested earlier, the visual and qualitative observations from fluorescence microscopy affirm the excellent disinfection capability of the Fe-TiO_2 nanomaterial, even with a real-life tap water sample.

4. CONCLUSIONS

Using a template-assisted sol−gel method, a Fe-doped TiO_2 nanopowder with a nominal Fe content of 2.5 wt % was produced. This mesoporous nanomaterial exhibited a high specific surface area, the presence of 100% anatase phase, and consisted of roundish nanoparticles with relatively uniform shape and size.

In terms of optical properties in the visible range resulting from Fe-doping, the Fe-TiO_2 nanoparticles were characterized by a bandgap of 2.80 eV, the presence of subsurface Fe^{2+} species, and some surface FeO_xH_y species that absorb at 500 nm.

The photocatalytic activity under visible light was tested for antibacterial effectiveness against the Gram-negative *E. coli* and the Gram-positive *S. aureus* bacteria in liquid media, at relatively high bacteria concentrations of 10^6 and 10^4 CFU/mL, using two concentrations of photocatalyst: 1 and 0.5 g/L. Consistent with the literature, 1 g/L proved to be the optimal concentration for the experimental conditions used.

Compared to undoped TiO_2 synthesized by the same method, the Fe-TiO_2 nanoparticles proved to be more effective, likely due to their optical properties. They facilitated the photocatalytic disinfection of both *E. coli* and *S. aureus* under visible light illumination produced by an inexpensive, commercially available LED lamp. The bacterial Log reduction of *E. coli* (3.57 ± 0.21 Log) and *S. aureus* (3.49 ± 0.42 Log) achieved with 1 g/L of nanomaterial after 240 min under visible light irradiation in liquid media was verified through live/dead fluorescence staining. Reusability tests demonstrated that the Fe-TiO_2 nanoparticles remained active for at least three cycles following the initial cycle, despite some limited Fe leaching.

The Fe-TiO_2 nanoparticles were also tested under the same optimal conditions (1 g/L powder concentration and visible light illumination) to eliminate microbial contamination in an actual tap water sample collected from a household in Jamshoro, Pakistan. Interestingly, the bacteria were photocatalytically inactivated within 30 min of exposure under visible light irradiation.

Without comprehensive guidelines on the conditions to be used during such tests, comparing data obtained with different types of illumination, reactor configurations, and nanomaterials is not straightforward. However, a comparison with previous literature regarding microbial contamination due to the photocatalytic activity of Fe-doped TiO_2 shows that the nanomaterial proposed here shows significant performance against high concentrations of both *E. coli* and *S. aureus* merely under visible light, which differs from most studies that focus on UV-light activation This suggests that the use of Fe-doped TiO_2 nanoparticles for photocatalytic water disinfection under visible light warrants further studies. To implement a Fe-doped TiO_2 photocatalyst in industrial or large-scale applications, producing 3D printed filters or membranes would benefit small and larger industries to inactivate pathogenic bacteria. These 3D filters and membranes can be utilized in the food industry, biomedical field, and water treatment. The advantages of these filters include sustainable recovery and recyclability options.

■ ASSOCIATED CONTENT

Supporting Information

The Supporting Information is available free of charge at https://pubs.acs.org/doi/10.1021/acsanm.5c01408.

Summary of key literature studies on photocatalytic bacterial disinfection using Fe-doped TiO_2 materials; water quality parameters of the contaminated tap water sample collected from a household in Jamshoro (Pakistan), and EDS and ICP-MS determined iron content in the Fe-TiO_2 nanopowder before after four photocatalytic cycles with *E. coli* and *S. aureus*; additional experimental data concerning FESEM images of the two studied nanomaterials; HR XP spectrum for the Fe 2p line of the Fe-TiO_2 nanopowder; selected HAADF maps and EDS spectra of the Fe-TiO_2 nanopowder before after four photocatalytic cycles with *E. coli* and *S. aureus*; selected representative images of *E. coli* and *S. aureus* bacterial counts (CFU/mL) obtained with an initial bacterial concentration of 10^6 CFU/mL under visible light irradiation in the presence of 1 g/L Fe-TiO_2, undoped TiO_2 and during control experiments; evaluation over time of the viable CFU/mL (Log scale) of *E. coli* and *S. aureus* obtained with an initial bacterial concentration of 10^6 CFU/mL in the presence of 0.5 g/L Fe-TiO_2 under visible light irradiation, during light control and dark control 1 experiments; evaluation over time of the viable CFU/mL (Log scale) of *E. coli* and *S. aureus* starting from an initial bacterial concentration of 10^4 CFU/mL under visible light irradiation in the presence of 0.5 g/L Fe-TiO_2, during light control and dark control 1 experiments; kinetic curves of *E. coli* and *S. aureus* under visible light irradiation in the presence of 0.5 and 1 g/L Fe-TiO_2 with initial bacteria concentrations of 10^6 CFU/mL and 10^4 CFU/mL; and optical microscope images of live/dead fluorescence staining related to the photocatalytic disinfection of *S. aureus* and of *E. coli* under visible light using 1 g/L Fe-TiO_2 with an initial bacteria concentration of 10^4 CFU/mL (PDF)

■ AUTHOR INFORMATION

Corresponding Author

Barbara Bonelli − *Department of Applied Science and Technology, INSTM-Unit of Torino Politecnico, and PolitoBIOMed Laboratory, Politecnico di Torino, 10129 Torino, Italy;* orcid.org/0000-0002-4716-864X; Email: barbara.bonelli@polito.it

Authors

Najeebullah Channa − *Department of Applied Science and Technology, Politecnico di Torino, 10129 Torino, Italy;* orcid.org/0000-0002-2542-4315

Tanveer A. Gadhi − *US Pakistan Center for Advanced Studies in Water (USPCASW), Mehran University of Engineering and Technology, Jamshoro 76062, Pakistan;* orcid.org/0000-0002-2544-4690

Francesca Stefania Freyria − *Department of Applied Science and Technology and INSTM-Unit of Torino Politecnico,*

https://doi.org/10.1021/acsanm.5c01408
ACS Appl. Nano Mater. 2025, 8, 10066−10079

Politecnico di Torino, 10129 Torino, Italy; orcid.org/0000-0002-2710-5545

Alessandro Chiadò − *Department of Applied Science and Technology and PolitoBIOMed Laboratory, Politecnico di Torino, 10129 Torino, Italy;* orcid.org/0000-0002-3230-8427

Nicola Blangetti − *Department of Applied Science and Technology, Politecnico di Torino, 10129 Torino, Italy;* orcid.org/0009-0001-4158-7253

Nicoletta Ditaranto − *Chemistry Department, Aldo Moro University of Bari, Bari 70126, Italy;* orcid.org/0000-0001-7529-9906

Complete contact information is available at: https://pubs.acs.org/10.1021/acsanm.5c01408

Author Contributions

All the authors have read and given approval to the final version of the manuscript. Conceptualization: B.B., T.A.G., A.C., N.C. Methodology: T.A.G., N.C., A.C., F.S.F. Samples characterization and analysis, Investigation: F.S.F., N.C., N.d.T. and N.B., T.A.G., Writing-original draft: N.C., B.B., F.St.F., T.A.G., A.C., N.d.T., Writing−Review editing: B.B., F.S.F., A.C., Supervision: B.B., T.A.G., A.C.

Funding

FSF contribution was carried out within the Agritech National Research Center and received funding from the European Union Next-GenerationEU (PIANO NAZIONALE DI RIPRESA E RESILIENZA (PNRR)−MISSIONE 4 COMPONENTE 2, INVESTIMENTO 1.4−D.D. 1032 17/06/2022, CN00000022). This manuscript reflects only the authors' views and opinions, neither the European Union nor the European Commission can be considered responsible for them. This study was carried out within the ≪GREEN UP: GREENER NANOMATERIALS FOR UPCONVERSION IN PHOTOCATALYTIC APPLICATIONS≫ project−funded by the Ministero dell'Università e della Ricerca−within the PRIN 2022 program (D.D.104 −02/02/2022) funded by the European Union − Next Generation EU. This manuscript reflects only the authors' views and opinions and the Ministry cannot be considered responsible for them.

Notes

The authors declare no competing financial interest.

■ ACKNOWLEDGMENTS

The authors thank Prof. Francesca Bosco and Dr. Chiara Mollea (from the Department of Applied Science and Technology at Politecnico di Torino) for the fruitful discussion; Dr Marco Allione (from the Department of Applied Science and Technology at Politecnico di Torino) for his assistance during HRTEM analyses; Drs. Carla Celozzi (from the Department of Applied Science and Technology at Politecnico di Torino) and Fabrizio Bianco (from the Department of Environment, Land and Infrastructure Engineering at Politecnico di Torino) for the ICP-MS analyses. The authors thank Dr. Kamran Ansari and Prof. Dr. Rasool Bux Mahar (the current and former director of USPCASW, MUET, Jamshoro, Pakistan) for their technical and administrative support during the bacterial inactivation experiments at USPCASW, Pakistan. The authors also acknowledge the support of the Higher Education Commission of Pakistan, provided through the laboratory infrastructure at USPCASW, MUET, managed under the funded research project COE-HEC-37. Some vector elements in Schemes 1 and 2, as well as the TOC, were designed by Freepik (www.freepik.com).

■ REFERENCES

(1) Khatri, N.; Tyagi, S. Influences of Natural and Anthropogenic Factors on Surface and Groundwater Quality in Rural and Urban Areas. *Front. Life Sci.* **2015**, *8* (1), 23−39.

(2) Sharma, S.; Bhattacharya, A. Drinking Water Contamination and Treatment Techniques. *Appl. Water Sci.* **2017**, *7* (3), 1043−1067.

(3) Olds, H. T.; Corsi, S. R.; Dila, D. K.; Halmo, K. M.; Bootsma, M. J.; McLellan, S. L. High Levels of Sewage Contamination Released from Urban Areas after Storm Events: A Quantitative Survey with Sewage Specific Bacterial Indicators. *PLOS Med.* **2018**, *15* (7), No. e1002614.

(4) Pinongcos, F.; Mladenov, N.; Calderon, J.; Verbyla, M. E.; Kinoshita, A. M.; Gersberg, R.; Batikian, C. M. Chemical and Microbial Markers for Discriminating Sanitary Sewer Contamination in Coastal. *Urban Streams. ACS ES&T Water* **2022**, *2* (10), 1747−1759.

(5) Ahmed, J.; Wong, L. P.; Chua, Y. P.; Yasmin, A.; Channa, N.; VanDerslice, J. A. Estimation of Hepatitis A Virus Infection Prevalence Through Drinking Water Supply of Primary Schools of Sindh, Pakistan. *Hepat. Mon.* **2020**, *20* (5), No. e98412.

(6) Ahmed, J.; Wong, L. P.; Chua, Y. P.; Channa, N. Drinking Water Quality Mapping Using Water Quality Index and Geospatial Analysis in Primary Schools of Pakistan. *Water* **2020**, *12* (12), 3382.

(7) Ahmed, J.; Wong, L. P.; Channa, N.; Ahmed, W.; Chua, Y. P.; Shaikh, M. Z. Arsenic Contamination and Potential Health Risk to Primary School Children through Drinking Water Sources. *Hum. Ecol. Risk Assess. An Int. J.* **2023**, *29* (2), 369−389.

(8) Ahmed, J.; Wong, L. P.; Chua, Y. P.; Channa, N.; Mahar, R. B.; Yasmin, A.; VanDerslice, J. A.; Garn, J. V. Quantitative Microbial Risk Assessment of Drinking Water Quality to Predict the Risk of Waterborne Diseases in Primary-School Children. *Int. J. Environ. Res. Public Health* **2020**, *17* (8), 2774.

(9) Saima, S.; Ferdous, J.; Sultana, R.; Rashid, R. Bin; Almeida, S.; Begum, A.; Jensen, P. K. M. Detecting Enteric Pathogens in Low-Risk Drinking Water in Dhaka, Bangladesh: An Assessment of the WHO Water Safety Categories. *Trop. Med. Infect. Dis.* **2023**, *8* (6), 321.

(10) Guo, L.; Wan, K.; Zhu, J.; Ye, C.; Chabi, K.; Yu, X. Detection and Distribution of Vbnc/Viable Pathogenic Bacteria in Full-Scale Drinking Water Treatment Plants. *J. Hazard. Mater.* **2021**, *406*, No. 124335.

(11) Al-Abri, M.; Al-Ghafri, B.; Bora, T.; Dobretsov, S.; Dutta, J.; Castelletto, S.; Rosa, L.; Boretti, A. Chlorination Disadvantages and Alternative Routes for Biofouling Control in Reverse Osmosis Desalination. *npj Clean Water 2019 21* **2019**, *2* (1), 1−16.

(12) Zhao, R.; Yang, X.-W.; Li, T.-H.; Yu, T.-M.; Chen, F.-Y.; Shen, Z.-R. The Application of Diatomic Catalysts in Advanced Oxidation Fenton-like Water Treatment Technology: A Mini Review. *Environ. Funct. Mater.* **2024**, *3* (1), 59−71.

(13) Ni, L.; Meng, J.; Li, X.; Zhang, Y. Surface Coating on the Polyamide TFC RO Membrane for Chlorine Resistance and Antifouling Performance Improvement. *J. Membr. Sci.* **2014**, *451*, 205−215.

(14) Li, X.-F.; Mitch, W. A. Drinking Water Disinfection Byproducts (DBPs) and Human Health Effects: Multidisciplinary Challenges and Opportunities. *Environ. Sci. Technol.* **2018**, *52* (4), 1681−1689.

(15) Helte, E.; Säve-Söderbergh, M.; Ugge, H.; Fall, K.; Larsson, S. C.; Åkesson, A. Chlorination By-Products in Drinking Water and Risk of Bladder Cancer−A Population-Based Cohort Study. *Water Res.* **2022**, *214*, No. 118202.

(16) Amalfitano, S.; Levantesi, C.; Garrelly, L.; Giacosa, D.; Bersani, F.; Rossetti, S. Water Quality and Total Microbial Load: A Double-Threshold Identification Procedure Intended for Space Applications. *Front. Microbiol.* **2018**, *9*, 416037.

(17) Ding, Y.; Yang, G.; Zheng, S.; Gao, X.; Xiang, Z.; Gao, M.; Wang, C.; Liu, M.; Zhong, J. Advanced Photocatalytic Disinfection

Mechanisms and Their Challenges. *J. Environ. Manage.* **2024**, *366*, No. 121875.
(18) Yang, G.; Yin, H.; Liu, W.; Yang, Y.; Zou, Q.; Luo, L.; Li, H.; Huo, Y.; Li, H. Synergistic Ag/TiO_2-N Photocatalytic System and Its Enhanced Antibacterial Activity towards Acinetobacter Baumannii. *Appl. Catal. B Environ.* **2018**, *224*, 175−182.
(19) Yang, G.; Wang, L.; Zhang, C.; Li, P.; Du, H.; Mao, Y.; Qiu, M.; Li, Q.; Hao, D.; Wang, Q. Novel Graphene Quantum Dots Modified NH_2-MIL-125 Photocatalytic Composites for Effective Antibacterial Property and Mechanism Insight. *Sep. Purif. Technol.* **2023**, *312*, No. 123433.
(20) Anucha, C. B.; Altin, I.; Bacaksiz, E.; Stathopoulos, V. N. Titanium Dioxide (TiO_2)-Based Photocatalyst Materials Activity Enhancement for Contaminants of Emerging Concern (CECs) Degradation: In the Light of Modification Strategies. *Chem. Eng. J. Adv.* **2022**, *10*, No. 100262.
(21) Foster, H. A.; Ditta, I. B.; Varghese, S.; Steele, A. Photocatalytic Disinfection Using Titanium Dioxide: Spectrum and Mechanism of Antimicrobial Activity. *Appl. Microbiol. Biotechnol. 2011 906* **2011**, *90* (6), 1847−1868.
(22) Zuo, G. M.; Cheng, Z. X.; Chen, H.; Li, G. W.; Miao, T. Study on Photocatalytic Degradation of Several Volatile Organic Compounds. *J. Hazard. Mater.* **2006**, *128* (2−3), 158−163.
(23) Blangetti, N.; Freyria, F. S.; Calviello, M. C.; Ditaranto, N.; Guastella, S.; Bonelli, B. Photocatalytic Degradation of Paracetamol under Simulated Sunlight by Four TiO_2 Commercial Powders: An Insight into the Performance of Two Sub-Micrometric Anatase and Rutile Powders and a Nanometric Brookite Powder. *Catalysts* **2023**, *13* (2), 434.
(24) Paleologou, A.; Marakas, H.; Xekoukoulotakis, N. P.; Moya, A.; Vergara, Y.; Kalogerakis, N.; Gikas, P.; Mantzavinos, D. Disinfection of Water and Wastewater by TiO_2 Photocatalysis, Sonolysis and UV-C Irradiation. *Catal. Today* **2007**, *129* (1−2), 136−142.
(25) Thakur, I.; Verma, A.; Örmeci, B. Visibly Active Fe-TiO_2 Composite: A Stable and Efficient Catalyst for the Catalytic Disinfection of Water Using a Once-through Reactor. *J. Environ. Chem. Eng.* **2021**, *9* (6), No. 106322.
(26) Gomathi Thanga Keerthana, B.; Murugakoothan, P. Synthesis and Characterization of CdS/TiO_2 Nanocomposite: Methylene Blue Adsorption and Enhanced Photocatalytic Activities. *Vacuum* **2019**, *159*, 476−481.
(27) Liu, X.; Xu, Y.; Zhong, Z.; Fu, Y.; Deng, Y. Preparation of Zn/TiO_2 Powder and Its Photocatalytic Performance for Oxidation of P-Nitrophenol. *Nucl. Sci. Technol.* **2007**, *18* (1), 59−64.
(28) Obregón, S.; Muñoz-Batista, M. J.; Fernández-García, M.; Kubacka, A.; Colón, G. Cu−TiO_2 Systems for the Photocatalytic H_2 Production: Influence of Structural and Surface Support Features. *Appl. Catal. B Environ.* **2015**, *179*, 468−478.
(29) Thakur, I.; Verma, A.; Örmeci, B. Fe−TiO_2 Composite Mediated the Hybrid Effect of Photocatalysis and Photo-Fenton for the Inactivation of Escherichia Coli Using a Continuous Flow Recirculation Reactor. *Ind. Eng. Chem. Res.* **2021**, *60* (20), 7558−7571.
(30) Taylor, K. G.; Konhauser, K. O. Iron in Earth Surface Systems: A Major Player in Chemical and Biological Processes. *Elements* **2011**, *7* (2), 83−88.
(31) Mancuso, A.; Sacco, O.; Vaiano, V.; Bonelli, B.; Esposito, S.; Freyria, F. S.; Blangetti, N.; Sannino, D. Visible Light-Driven Photocatalytic Activity and Kinetics of Fe-Doped TiO_2 Prepared by a Three-Block Copolymer Templating Approach. *Materials (Basel).* **2021**, *14* (11), 3105.
(32) Freyria, F.; Compagnoni, M.; Ditaranto, N.; Rossetti, I.; Piumetti, M.; Ramis, G.; Bonelli, B. Pure and Fe-Doped Mesoporous Titania Catalyse the Oxidation of Acid Orange 7 by H_2O_2 under Different Illumination Conditions: Fe Doping Improves Photocatalytic Activity under Simulated Solar Light. *Catalysts* **2017**, *7* (7), 213.
(33) Piumetti, M.; Freyria, F. S.; Armandi, M.; Geobaldo, F.; Garrone, E.; Bonelli, B. Fe- and V-Doped Mesoporous Titania Prepared by Direct Synthesis: Characterization and Role in the Oxidation of AO7 by H_2O_2 in the Dark. *Catal. Today* **2014**, *227*, 71−79.
(34) Khan, M. S.; Shah, J. A.; Riaz, N.; Butt, T. A.; Khan, A. J.; Khalifa, W.; Gasmi, H. H.; Latifee, E. R.; Arshad, M.; Al-Naghi, A. A. A.; Ul-Hamid, A.; Arshad, M.; Bilal, M. Synthesis and Characterization of Fe-TiO_2 Nanomaterial: Performance Evaluation for RB5 Decolorization and In Vitro Antibacterial Studies. *Nanomater. 2021, Vol. 11, Page 436* **2021**, *11* (2), 436.
(35) Meng, D.; Liu, X.; Xie, Y.; Du, Y.; Yang, Y.; Xiao, C. Antibacterial Activity of Visible Light-Activated TiO_2 Thin Films with Low Level of Fe Doping. *Adv. Mater. Sci. Eng.* **2019**, *2019*, 1−8.
(36) Park, B.; Nizet, V.; Liu, G. Y. Role of Staphylococcus Aureus Catalase in Niche Competition against Streptococcus Pneumoniae. *J. Bacteriol.* **2008**, *190* (7), 2275−2278.
(37) O'Riordan, K.; Lee, J. C. Staphylococcus Aureus Capsular Polysaccharides. *Clin. Microbiol. Rev.* **2004**, *17* (1), 218−234.
(38) Yadav, H. M.; Kolekar, T. V.; Pawar, S. H.; Kim, J. S. Enhanced Photocatalytic Inactivation of Bacteria on Fe-Containing TiO_2 Nanoparticles under Fluorescent Light. *J. Mater. Sci.: Mater. Med.* **2016**, *27* (3), 57.
(39) Poostforooshan, J.; Belbekhouche, S.; Olszok, V.; Stodt, M. F. B.; Simmler, M.; Bierwirth, M.; Nirschl, H.; Kiefer, J.; Fritsching, U.; Weber, A. P. Synthesis of Pure and Fe-Doped TiO_2 Nanoparticles via Electrospray-Assisted Flame Spray Pyrolysis for Antimicrobial Applications. *ACS Appl. Nano Mater.* **2023**, *6* (24), 22660−22672.
(40) Kamble, R. J.; Gaikwad, P. V. Peroxy Titanium Complex Derived Fe-Doped TiO_2 Nanoparticles: Synthesis, Properties and Antibacterial Activity. *Mater. Today Proc.* **2021**, *45*, 3784−3788.
(41) Koli, V. B.; Delekar, S. D.; Pawar, S. H. Photoinactivation of Bacteria by Using Fe-Doped TiO_2-MWCNTs Nanocomposites. *J. Mater. Sci. Mater. Med.* **2016**, *27* (12), 177.
(42) Baruah, M.; Ezung, S. L.; Supong, A.; Bhomick, P. C.; Kumar, S.; Sinha, D. Synthesis, Characterization of Novel Fe-Doped TiO_2 Activated Carbon Nanocomposite towards Photocatalytic Degradation of Congo Red, E. Coli, and S. Aureus. *Korean J. Chem. Eng.* **2021**, *38* (6), 1277−1290.
(43) Yin, J.; Lv, L.; Chu, Y.; Tan, L. Highly Antibacterial Cu/Fe/N Co-Doped TiO_2 Nanopowder under Visible Light. *Inorg. Chem. Commun.* **2023**, *151*, No. 110587.
(44) Schlur, L.; Begin-Colin, S.; Gilliot, P.; Gallart, M.; Carré, G.; Zafeiratos, S.; Keller, N.; Keller, V.; André, P.; Greneche, J.-M.; Hezard, B.; Desmonts, M.-H.; Pourroy, G. Effect of Ball-Milling and Fe-/Al-Doping on the Structural Aspect and Visible Light Photocatalytic Activity of TiO_2 towards Escherichia Coli Bacteria Abatement. *Mater. Sci. Eng., C* **2014**, *38* (1), 11−19.
(45) Feilizadeh, M.; Mul, G.; Vossoughi, M. E. Coli Inactivation by Visible Light Irradiation Using a Fe−Cd/TiO_2 Photocatalyst: Statistical Analysis and Optimization of Operating Parameters. *Appl. Catal. B Environ.* **2015**, *168−169*, 441−447.
(46) Arellano, U.; Asomoza, M.; Ramírez, F. Antimicrobial Activity of Fe−TiO_2 Thin Film Photocatalysts. *J. Photochem. Photobiol. A Chem.* **2011**, *222* (1), 159−165.
(47) Ang, J. K. K.; Chua, J. S. M.; Chang, Z. J.; Li, Z.; Bai, H.; Sun, D. D. An Ion Exchange Approach Assembled Multi-Dimensional Hierarchical Fe−TiO_2 Composite Micro-/Nano Multi-Shell Hollow Spheres for Bacteria Lysis through Utilizing Visible Light. *Catal. Sci. Technol.* **2018**, *8* (8), 2077−2086.
(48) Al-Jawad, S. M. H.; Taha, A. A.; Salim, M. M. Synthesis and Characterization of Pure and Fe Doped TiO_2 Thin Films for Antimicrobial Activity. *Optik (Stuttg).* **2017**, *142*, 42−53.
(49) Azad, A.; Hershey, R.; Ali, S.; Goel, V. Bactericidal Efficacy of Electrospun Pure and Fe-Doped Titania Nanofibers. *J. Mater. Res.* **2010**, *25* (9), 1761−1770.
(50) Manzoli, M.; Freyria, F. S.; Blangetti, N.; Bonelli, B. Brookite, a Sometimes under Evaluated TiO_2 Polymorph. *RSC Adv.* **2022**, *12* (6), 3322−3334.
(51) Jütte, M.; Abdighahroudi, M. S.; Waldminghaus, T.; Lackner, S.; Lutze, V.; H. Bacterial Inactivation Processes in Water

https://doi.org/10.1021/acsanm.5c01408
ACS Appl. Nano Mater. 2025, 8, 10066−10079

Disinfection−Mechanistic Aspects of Primary and Secondary Oxidants−A Critical Review. *Water Res.* **2023**, *231*, No. 119626.
(52) Palková, Z. Multicellular Microorganisms: Laboratory versus Nature. *EMBO Rep.* **2004**, *5* (5), 470−476.
(53) Birben, N. C.; Lale, E.; Pelosato, R.; Turkten, N.; Sora, I. N.; Bekbolet, M. Photocatalytic Bactericidal Performance of $LaFeO_3$ under Solar Light in the Presence of Natural Organic Matter: Spectroscopic and Mechanistic Evaluation. *Water* **2021**, *13* (19), 2785.
(54) Wamyil, J. F.; Chukwuanugo Nkemakonam, O.; Adewale, O. S.; Nabona, J.; Ntulume, I.; Wamyil, F. B. Microbiological Quality of Water Samples Obtained from Water Sources in Ishaka. *Uganda. SAGE Open Med.* **2023**, *11*, 1−8.
(55) Tzeng, J.-H.; Weng, C.-H.; Yen, L.-T.; Gaybullaev, G.; Chang, C.-J.; de Luna, M. D. G.; Lin, Y.-T. Inactivation of Pathogens by Visible Light Photocatalysis with Nitrogen-Doped TiO_2 and Tourmaline-Nitrogen Co-Doped TiO_2. *Sep. Purif. Technol.* **2021**, *274*, No. 118979.
(56) Baudišová, D. Evaluation of Escherichia Coli as the Main Indicator of Faecal Pollution. *Water Sci. Technol.* **1997**, *35* (11−12), 333−336.
(57) Devane, M. L.; Moriarty, E.; Weaver, L.; Cookson, A.; Gilpin, B. Fecal Indicator Bacteria from Environmental Sources; Strategies for Identification to Improve Water Quality Monitoring. *Water Res.* **2020**, *185*, No. 116204.
(58) Hazan, R.; Que, Y. A.; Maura, D.; Rahme, L. G. A Method for High Throughput Determination of Viable Bacteria Cell Counts in 96-Well Plates. *BMC Microbiol.* **2012**, *12* (1), 259.
(59) Yen, L. T.; Weng, C. H.; Than, N. A. T.; Tzeng, J. H.; Jacobson, A. R.; Iamsaard, K.; Dang, V. D.; Lin, Y. T. Mode of Inactivation of Staphylococcus Aureus and Escherichia Coli by Heated Oyster-Shell Powder. *Chem. Eng. J.* **2022**, *432*, No. 134386.
(60) Campbell, L.; Nguyen, S. H.; Webb, H. K.; Eldridge, D. S. Photocatalytic Disinfection of S. Aureus Using Black TiO_{2-x} under Visible Light. *Catal. Sci. Technol.* **2023**, *13* (1), 62−71.
(61) Channa, N.; Gadhi, T. A.; Mahar, R. B.; Chiadò, A.; Bonelli, B.; Tagliaferro, A. Combined Photocatalytic Degradation of Pollutants and Inactivation of Waterborne Pathogens Using Solar Light Active α/β-Bi_2O_3. *Colloids Surfaces A Physicochem. Eng. Asp.* **2021**, *615*, No. 126214.
(62) Das, S.; Ranjana, N.; Misra, A. J.; Suar, M.; Mishra, A.; Tamhankar, A. J.; Lundborg, C. S.; Tripathy, S. K. Disinfection of the Water Borne Pathogens Escherichia Coli and Staphylococcus Aureus by Solar Photocatalysis Using Sonochemically Synthesized Reusable Ag@ZnO Core-Shell Nanoparticles. *Int. J. Environ. Res. Public Heal. 2017, Vol. 14, Page 747* **2017**, *14* (7), 747.
(63) Walter, W. G. Standard Methods For The Examination Of Water And Wastewater. In *American Journal of Public Health and the Nations Health*, 11th ed.; American Public Health Association, 1961; Vol. *51*, pp 940−940.
(64) Lauer, W. F.; Martinez, F. L.; Patel, A. Validation of RAPID'E. Coli 2 for Enumeration and Differentiation of Escherichia Coli and Other Coliform Bacteria in Selected FoodsPerformance-Tested MethodSM 050601. *J. AOAC Int.* **2007**, *90* (5), 1284−1315.
(65) Armandi, M.; Bonelli, B.; Karaindrou, E. I.; Areán, C. O.; Garrone, E. Post-Synthesis Modifications of SBA-15 Carbon Replicas: Improving Hydrogen Storage by Increasing Microporous Volume. *Catal. Today* **2008**, *138* (3−4), 244−248.
(66) Bapna, K.; Phase, D. M.; Choudhary, R. J. Study of Valence Band Structure of Fe Doped Anatase TiO_2 Thin Films. *J. Appl. Phys.* **2011**, *110* (4), 43910.
(67) Grosvenor, A. P.; Kobe, B. A.; Biesinger, M. C.; McIntyre, N. S. Investigation of Multiplet Splitting of Fe 2p XPS Spectra and Bonding in Iron Compounds. *Surf. Interface Anal.* **2004**, *36* (12), 1564−1574.
(68) Paiva, C. N.; Bozza, M. T. Are Reactive Oxygen Species Always Detrimental to Pathogens? *Antioxid. Redox Signal.* **2014**, *20* (6), 1000−1034.
(69) Perry, C. C.; Weatherly, M.; Beale, T.; Randriamahefa, A. Atomic Force Microscopy Study of the Antimicrobial Activity of Aqueous Garlic versus Ampicillin against Escherichia Coli and Staphylococcus Aureus. *J. Sci. Food Agric.* **2009**, *89* (6), 958−964.
(70) Ahmed, J.; Wong, L. P.; Chua, Y. P.; Channa, N.; Memon, U.-R.; Garn, J. V.; Yasmin, A.; VanDerslice, J. A. Heavy Metals Drinking Water Contamination and Health Risk Assessment among Primary School Children of Pakistan. *J. Environ. Sci. Heal. Part A* **2021**, *56* (6), 667−679.

https://doi.org/10.1021/acsanm.5c01408
ACS Appl. Nano Mater. 2025, 8, 10066−10079